Bioactive Materials 19 (2023) 418–428

Contents lists available at ScienceDirect

Bioactive Materials

journal homepage: www.keaipublishing.com/en/journals/bioactive-materials

Extracellular magnetic labeling of biomimetic hydrogel-induced human mesenchymal stem cell spheroids with ferumoxytol for MRI tracking

Sen Yan [a], Ke Hu [b,c], Miao Zhang [a], Jingyi Sheng [a], Xueqin Xu [b], Shijia Tang [c], Yan Li [a], Sheng Yang [d], Guangxiang Si [a], Yu Mao [a], Yi Zhang [e], Feimin Zhang [c,**], Ning Gu [a,*]

[a] State Key Laboratory of Bioelectronics, Jiangsu Key Laboratory for Biomaterials and Devices, School of Biological Science and Medical Engineering, Southeast University, Nanjing, 210009, Jiangsu, China
[b] Laboratory of Oral Regenerative Medicine Technology, School of Biomedical Engineering and Informatics, Department of Biomedical Engineering, Nanjing Medical University, Nanjing, 211166, Jiangsu, China
[c] Jiangsu Key Laboratory of Oral Diseases, Affiliated Hospital of Stomatology, Nanjing Medical University, Nanjing, 210029, Jiangsu, China
[d] Department of Biomedical Engineering, School of Medicine, Tsinghua University, Beijing, 100084, China
[e] Department of Colorectal Surgery, The First Affiliated Hospital of Nanjing Medical University, Nanjing, 210000, Jiangsu, China

ARTICLE INFO

Keywords:
Superparamagnetic iron oxide nanoparticles
MSC labeling
Mechanically tunable biomimetic hydrogel
Spheroids
MRI tracking

ABSTRACT

Labeling of mesenchymal stem cells (MSCs) with superparamagnetic iron oxide nanoparticles (SPIONs) has emerged as a potential method for magnetic resonance imaging (MRI) tracking of transplanted cells in tissue repair studies and clinical trials. Labeling of MSCs using clinically approved SPIONs (ferumoxytol) requires the use of transfection reagents or magnetic field, which largely limits their clinical application. To overcome this obstacle, we established a novel and highly effective method for magnetic labeling of MSC spheroids using ferumoxytol. Unlike conventional methods, ferumoxytol labeling was done in the formation of a mechanically tunable biomimetic hydrogel-induced MSC spheroids. Moreover, the labeled MSC spheroids exhibited strong MRI T2 signals and good biosafety. Strikingly, the encapsulated ferumoxytol was localized in the extracellular matrix (ECM) of the spheroids instead of the cytoplasm, minimizing the cytotoxicity of ferumoxytol and maintaining the viability and stemness properties of biomimetic hydrogel-induced MSC spheroids. This demonstrates the potential of this method for post-transplantation MRI tracking in the clinic.

1. Introduction

Mesenchymal stem cells (MSCs), which have self-renewal, differentiation and paracrine secretion abilities [1–3], have been widely used in research for the treatment of various diseases such as Alzheimer's disease, Parkinson's disease, spinal cord injury, osteoarthritis, and diabetes [4–8]. MSC therapy has shown significant potential in the field of regenerative medicine [9]. Currently, MSC therapies mainly involve intravenous administration, localized lesion transplantation, tissue engineering scaffold-based repair and organoid construction [10–14]. Successful MSC transplantation is a prerequisite for satisfactory therapeutic outcomes; however, the localization and fate of MSCs after transplantation is largely unknown due to the lack of reliable cell tracking technology.

Superparamagnetic iron oxide particles (SPIONs) have been widely used as cell labeling agents for MRI tracking in tissue repair studies and clinical trials [15–19], which usually requires passive labeling of nanoparticles by MSCs to shorten the lateral relaxation time during MRI via the superparamagnetism of the cells and produce dark contrast in T2-weighted MRI images [20–22]. The stability, solubility and biocompatibility of SPIONs are influenced by the polymer coatings [23]. Meanwhile the different coatings influence the internalization of SPIONs by MSCs, which related with the MRI sensitivity after cell labeling [21,23]. Ferumoxytol (FMT), an FDA-approved nanoparticle for the treatment of iron deficiency anemia [24], is composed of a γ-Fe_2O_3 core and polyglucose sorbitol carboxymethylether (PSC) coating, and its stability and safety are widely recognized. As demonstrated by numerous studies, the cell labeling efficiency of ferumoxytol is very low. Cell labeling with

Peer review under responsibility of KeAi Communications Co., Ltd.
* Corresponding author.
** Corresponding author.
E-mail addresses: fmzhang@njmu.edu.cn (F. Zhang), guning@seu.edu.cn (N. Gu).

https://doi.org/10.1016/j.bioactmat.2022.04.024
Received 19 February 2022; Received in revised form 20 April 2022; Accepted 24 April 2022

ferumoxytol usually requires high labeling concentrations and the use of potentially toxic cationic transfection reagents such as poly-L-lysine and protamine sulfate, or magnetic field to improve uptake by MSCs, which also limits its clinical application [20,25–29]. In addition, the potential impact of prolonged accumulation of ferumoxytol inside MSCs has not been well investigated and needs to be thoroughly evaluated [30–32].

Distinct from traditional 2D culture, *in vitro* 3D culture of multicellular aggregates has been developed for decades. *In vitro* 3D culture of MSCs has also been developed for many years. Due to their spherical shape, these multicellular aggregates are now referred to as multicellular spheroids [33]. MSC spheroids have been used in the repair of a variety of tissues and organs [33,34]. Numerous studies have shown that, compared with conventional cell culture methods using culture dishes, culturing of 3D MSC spheroids *in vitro* can significantly improve the directional differentiation, homing, anti-inflammatory, and paracrine capacities of MSCs [35–38]. However, the application of spheroids faces the following challenges: differences in spheroids prepared by various 3D culture methods and a lack of effective methods for tracking spheroids after transplantation. 3D culture techniques usually include scaffold-free 3D culture methods and the use of bioscaffold materials such as hydrogels [39]. Recent studies have demonstrated that cell self-organization and spheroid formation can be achieved by modulating

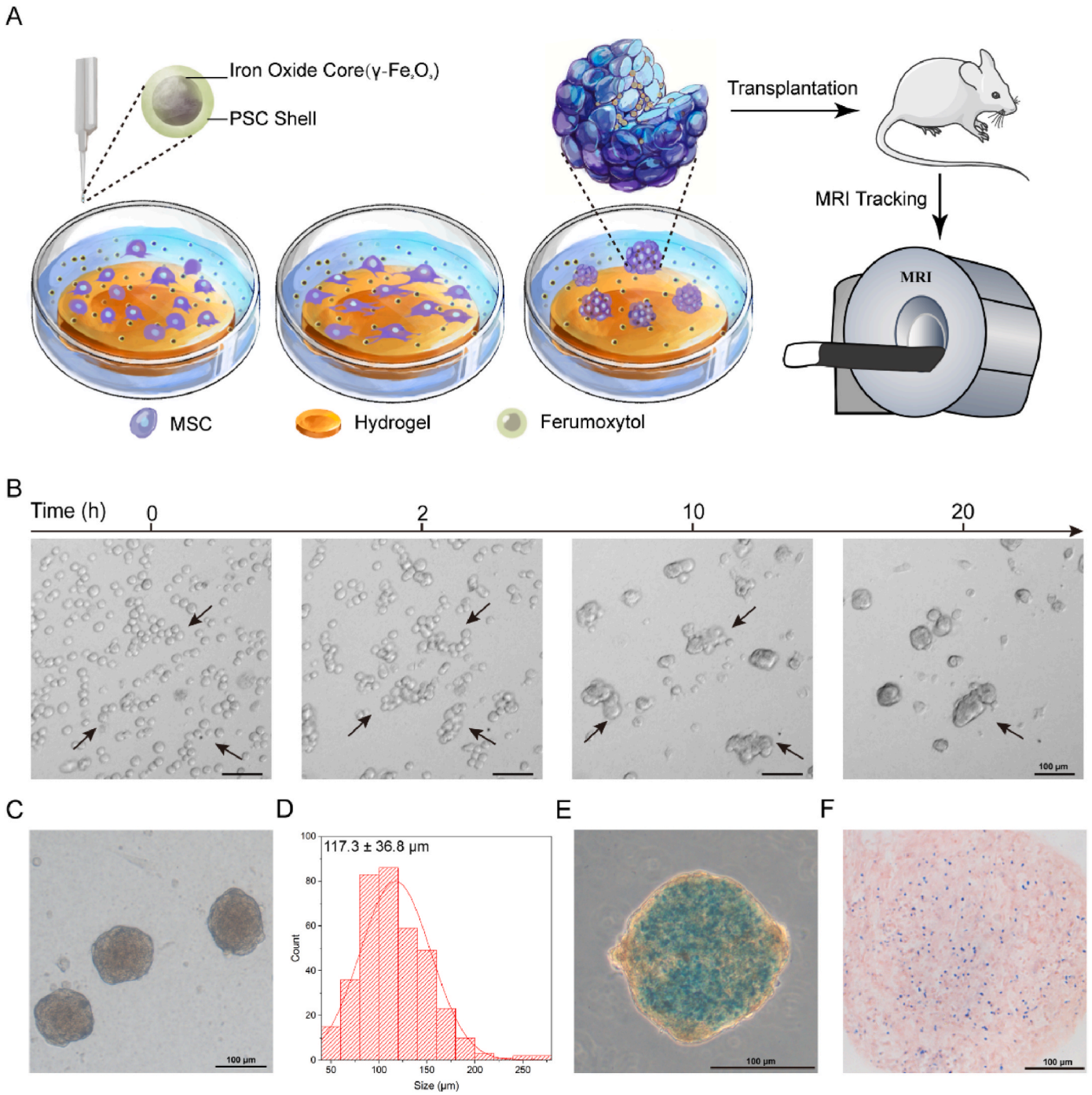

Fig. 1. HUC-MSC spheroids were labeled with ferumoxytol. (A) Schematic of ferumoxytol labeling of hUC-MSC spheroids. (B) Microscopy images of cells seeded on MCS-culturing hydrogel. (C) Morphology of hUC-MSC spheroids cultured for 3 days and (D) the size distribution of the spheroids. (E–F) Perls' staining of labeled hUC-MSC spheroids and cryosections.

the physical properties of cell culture environment, showing some advantages in simulating the *in vivo* microenvironment and improving spheroid function both *in vitro* and *in vivo*, such as the construction of tumor-like tissues, enhancing insulin secretion from pancreatic islet cells, and regulating the fate and activity of MSCs [40–42]. MSC spheroids-based cell therapy have been used for a variety of preclinical animal models [43]. Post-transplant MRI tracing can be used to determine whether transplantation was successful and evaluate the location or retention time of spheroids in damaged tissues [44,45]. Current studies for labeling spheroids or cell containing aggregates implanted *in vivo* still rely on the internalization of SPIONs by MSCs, which has low labeling efficiency and potential toxicity [46,47]. Therefore, the development of a safe and highly effective method for spheroid labeling is desirable.

In this study, we developed a magnetic labeling method that does not rely on the uptake of ferumoxytol, thus simplifying the labeling process and reducing the cytotoxicity caused by the uptake of magnetic nanoparticles. We showed that MSC spheroids with complex network structures can be directly labeled by encapsulating ferumoxytol into the spheroids (Fig. 1A). Our results suggest that during cellular self-organization and spheroid formation induced by a biomimetic hydrogel, ferumoxytol can be encapsulated into spheroids by binding with abundant extracellular matrix (ECM) proteins in the spheroids, ultimately allowing effective MRI tracking of MSC spheroids after transplantation. This novel approach involves the use of ferumoxytol without the employment of additional transfection reagents, improving its clinical translation. In addition, this labeling method does not rely on the cellular uptake of ferumoxytol, eliminating the potential cytotoxic effects of this process. In conclusion, our study provides an alternative strategy for safer and more effective MSC tracking, which is of great importance for stem cell transplantation.

2. Materials and methods

Preparation of the GelMA/PEGDA composite biomimetic hydrogel. Hydrogels with different mechanical properties were prepared by adjusting the composition of two monomers and the cross-linker. For stem cell MCS-culturing hydrogels, PEGDA (30 mg), N, N′-methylene-bis-acrylamide (0.05% wt.), and GelMA (80 mg) were added to 1 mL of ultrapure water and dissolved at 50 °C for 2 h, while for MLC-culturing hydrogels, PEGDA (10 mg), N,N′-methylene-bis-acrylamide (0.2% wt.), and GelMA (80 mg) were added to 1 mL of ultrapure water and dissolved at 50 °C for 2 h. LAP (5 mg) was added to the monomer solutions and dissolved for 5 min. Then, the abovementioned solutions were poured into a customized cylindrical mold (inner diameter: 30 mm; thickness: 1 mm) and exposed to visible light (405 nm) for 10 s for polymerization. The prepared composite hydrogels were rinsed with ultrapure water for 3 days. After sterilization with ethylene oxide, the hydrogels were applied as cell culture substrates.

Measurement of the mechanical properties of the biomimetic hydrogels. The Young's modulus and relaxation time of the biomimetic hydrogel were determined with a Piuma nanoindenter (Optics 11, Piuma, The Netherlands). The optical probe of the nanoindenter was spherical with a stiffness of 40.7 N m^{-1} and a tip radius of 24 μm. When measuring Young's modulus, the probe was set to indent the hydrogel 10 μm over 2 s and unloaded after holding for 1 s. When measuring the stress relaxation, the probe was set to indent the hydrogel 15 μm over 5 s and unloaded after holding for 600 s.

Cell culture. Human umbilical cord mesenchymal stem cells (hUC-MSCs) were obtained from the Clinical Stem Cell Center of the Nanjing Drum Tower Hospital (China). The hUC-MSCs were cultured with low glucose Dulbecco's modified Eagle's medium (L-DMEM, Gibco, USA) with 10% fetal bovine serum (FBS, Gibco, USA) and 1% penicillin and streptomycin (Gibco, USA) at 37 °C in a humidified 5% CO2 incubator. The medium was replaced every 3 days. For 3D culture and cell labeling, hUC-MSCs were harvested with (0.25% w/v) trypsin-EDTA (Gibco, USA) and seeded on hydrogels at a density of 1×10^5 cells per cm^2 with different concentrations of ferumoxytol. Ferumoxytol (γ-Fe_2O_3@PSC) was supplied by CTTQ Pharma (Nanjing, China) and possesses good monodispersity and dimensional homogeneity. The average size of iron-core was 7.49 ± 0.82 nm measured by Transmission Electron Microscopy (TEM; JEM-2100, Japan) which was showed in Fig. S1.

Perls' Staining. hUC-MSCs and spheroids were washed three times before being fixed in 4% paraformaldehyde at 4 °C for 30 min. To examine the labeling efficiency of ferumoxytol, Perls' staining solution and an equal volume of hydrochloric acid and potassium ferrocyanide (Sigma-Aldrich, USA) was used to detect iron, and then the spheroids were imaged by microscopy (Axiovert 200, Zeiss, Germany).

Iron Content Measurement by ICP-MS. To accurately quantify the labeling efficiency at different concentrations of ferumoxytol, iron content in the spheroids was measured by ICP-MS according to the operating procedures provided by PerkinElmer. In brief, spheroids labeled with ferumoxytol were first collected in a 15 mL centrifuge tube and washed with PBS three times. Then, the centrifuge tube was centrifuged at 2500 rpm for 5 min, and the PBS was removed. Then, 200 μL of 67% nitric acid was added, and the tube was kept in a water bath at 90 °C overnight to ensure that ferumoxytol was completely digested into Fe ions. Finally, the digested solution was diluted with deionized water, and the iron content was determined by ICP-MS (NexION 2000, PerkinElmer, USA). The iron content in the spheroids was normalized to the protein content.

TEM examination of cells. Spheroids labeled with ferumoxytol were harvested, centrifuged at 1500 rpm for 5 min and fixed overnight with 2.5% glutaraldehyde at 4 °C. The cell pellet then in 1% osmium tetroxide, dehydrated in ethanol, and embedded in epoxy resin (Sigma-Aldrich, USA) to obtain ultrathin sections. Finally, the sections were stained with lead citrate and uranyl acetate. All sections were imaged by TEM (JEM-200CX, JEOL, Japan) and analyzed using ImageJ.

Confocal imaging. hUC-MSC spheroids cultured on hydrogels were fixed in 4% paraformaldehyde for 1 h at 4 °C, permeabilized, and blocked with 0.3% NP–40/3% BSA in PBS for 30 min at room temperature. For primary antibody incubation, the following antibodies were used: rabbit anti-Col-I (1:500, Abcam), rabbit anti-fibronectin (1:200, Abcam), mouse *anti*-E-cadherin (1:100, Cell Signaling Technology), and mouse *anti*-N-cadherin (1:200, Abcam). The secondary antibodies were Alexa Fluor®488-conjugated donkey anti-mouse and Alexa Fluor®594-conjugated donkey anti-rabbit (1:200, Invitrogen). The nuclei were stained using mounting medium with DAPI (Sigma-Aldrich, USA). The viability of spheroids was assessed using the LIVE/DEAD™ Cell Imaging Kit (488/570) (Invitrogen, USA) according to the manufacturer's protocol. hUC-MSC spheroids were incubated with working reagents for 30 min at room temperature. Fluorescence images were acquired using a confocal laser scanning microscope (C2 Plus CLSM, Nikon, Japan).

Histological Analysis. Spheroids were collected in Eppendorf tubes and fixed in 4% paraformaldehyde at 4 °C for 1 h. After fixation, the spheroids were dehydrated in 30% sucrose and embedded in optimal cutting temperature media. Cryosections were cut at a thickness of 6 μm and stored at −80 °C. Immunofluorescence analysis and Perls' staining of cryosections was performed following previously described methods, and image analysis was performed with ImageJ.

Cell viability assay. *In vitro* cell viability was measured by the CCK-8 assay following to the manufacturer's instructions (Dojindo, Japan). The cell viability of hUC-MSCs cultured in complete medium supplemented with various concentrations of ferumoxytol for different durations were measured during the labeling process. *In vivo* cell viability was measured by TUNEL staining following to the protocol provided by manufacturer (Beyotime, China). Briefly, Cryosections of grafts were fixed in 4% paraformaldehyde at 4 °C for 30 min. The fixed sections were washed with PBS twice and incubated with 0.5% Triton X-100/PBS for 5 min. Then, samples were incubated with TUNEL staining solution at 37 °C for 1 h. Finally, cryosections were incubated with DAPI for 10 min at room temperature and acquired images by fluorescence

microscope (Ts-2R, Nikon, Japan).

Flow cytometry analysis. hUC-MSCs were identified, and apoptosis and ROS levels were measured using flow cytometry. Positive expression of MSC markers (detected with CD44-PE, CD73-PE, CD90-PE, CD105-PE) and negative expression markers (detected with CD14-FITC, CD19-FITC, CD34-FITC, CD45-FITC, HLA-DQ-PE, HLA-DR-FIT) (BD Bioscience, USA) were used to identify hUC-MSCs by flow cytometry (Becton-Dickinson Accuri C6, BD Bioscience, USA). Isotype control antibodies were used for each experiment. The charts were graphed by FSC vs SSC. Apoptosis and ROS levels were determined by utilizing Annexin V/PI and DCFH-DA fluorescent probes (Invitrogen, USA). All data analysis was performed with FlowJo software.

Quantitative real-time PCR (qRT-PCR). Total RNA was isolated from spheroids using TRIzol reagent (Invitrogen, USA) following the manufacturer's protocol. Reverse transcription of 1 μg of total RNA was performed using HiScript III RT SuperMix for qPCR (Vazyme, China). qRT-PCR was performed with AceQ qPCR SYBR Green Master Mix (Vazyme, China) on a LightCycler 96 instrument (Roche). Relative expression was calculated using the $2^{-\Delta\Delta Ct}$ method and normalized to the expression of GAPDH. Each experiment was repeated at least three times and each sample was analyzed in triplicate. The specific primer sequences used are listed in Table S1.

Western blot analysis. MSC spheroids were harvested and lysed in RIPA buffer (50 mmol L^{-1} Tris-HCl pH8.0, 150 mmol L^{-1} NaCl, 1% TritonX-100, 100 μg mL^{-1} PMSF, and protease inhibitor cocktail) on ice for 30 min. The lysate was clarified by centrifugation for 20 min at 14,000 rpm at 4 °C. Equal amounts of protein (20 μg) were loaded onto a 10% SDS-PAGE gel, followed by western blotting with indicated antibodies. The blots were visualized using an enhanced chemiluminescence detection system. The primary antibodies used were *anti*-GAPDH (Proteintech, 10494-1-AP), anti-SOX2 (Abcam, ab92494), *anti*-Nanog (Abcam, ab109250), *anti*-Oct 4 (Abcam, ab181557).

CFU–F assay. hUC-MSCs from monolayers, spheroids and ferumoxytol-labeled spheroids were trypsinized into single cells and reseeded in 6 cm culture dishes at a density of 750 cells per dish. After culture for 21 days, the colonies were stained with crystal violet solution and counted to analyze the self-renewal capacity of the cells.

Evaluation of three lineages differentiation. To evaluate the osteogenic and adipogenic differentiation abilities of 2D-cultured hUC-MSCs, hUC-MSC spheroids and ferumoxytol-labeled spheroids, spheroids were trypsinized into single cells and seeded in 6-well culture plates at a density of 2×10^4 cells per cm^2. Following incubation for 1 day in complete medium, the cells were cultured in osteogenic and adipogenic differentiation culture medium. The osteogenic differentiation medium comprised complete culture media, 10 mM glycerol-2-phosphate, 50 μM L-ascorbic acid, and 100 nM dexamethasone. The adipogenic differentiation medium contained 10 μM insulin, 0.5 mM isobutylmethylxanthine, 1 μM dexamethasone, and 200 μM indomethacin (all from Sigma-Aldrich, USA). After culturing for 21 days, the cells were stained with alizarin red and Oil Red O. Differentiation efficiency was quantified by analyzed the percentage of staining-positive regions by ImageJ software. For chondrogenic differentiation, 3×10^5 2D-cultured cells and spheroids containing 3×10^5 cells were transferred to 15 mL centrifuge tube with chondrogenic differentiation medium contained ITS, 50 mg/mL ascorbic acid, 40 mg/ml L-Proline, 0.1 mM dexamethasone, and 10 ng/mL TGF-β3 (R&D, USA). On day 21, pellets were harvested for histology to detect sulfated glycosaminoglycan via Alcian Blue staining and analyzed the intensity of staining by ImageJ software.

***In vitro* MRI.** Labeled cells were collected, fixed in 4% paraformaldehyde solution for 30 min and resuspended in 100 μL PBS. Then, the cells were mixed with 100 μL 2% agarose and layered in an Eppendorf tube. The agarose cell layers were spaced using pure 2% agarose without cells. *I*n vitro T2-weighted MRI was then performed using a 7.0 T MRI instrument (Bruker Pharmascan, Germany). The parameters for T2-weighted scan were set as repetition time (TR) = 4390.34 ms, echo time (TE) = 33 ms, number of average = 1, flip angle = 135 deg. All images were obtained with a matrix size of 256 × 256, slice thickness of 1 mm and field of view (FOV) of 60 × 60 mm. Relative quantitative analysis of the signals was performed using ImageJ software.

***In vivo* MRI.** All *in vivo* experiments were performed according to the guidelines of the Animal Care & Welfare Committee of Southeast University (No. 20210526003). Then, 100 μL hUC-MSC spheroids containing 1×10^6 cells were prelabeled with DiI for 20 min according to the manufacturer's protocol (Beyotime, China) and mixed with 100 μL Matrigel (Corning, USA). Then, the mixture was subcutaneously injected into the right subaxillae of BALB/c nude mice. *In vivo* MRI was then conducted on a PharmaScan 7.0 T system (BioSpin MRI GmbH Bruker, Germany). The mice were anesthetized with isoflurane (1.5 vol%) via a nose cone. Body temperature was maintained at 37 °C. A two-dimensional RARE (pvm) sequence with respiratory gating control was employed. The parameters for T2-weighted scan were set as repetition time (TR) = 2500 ms, echo time (TE) = 33 ms, number of average = 3, flip angle = 180 deg. Axial images were obtained with a matrix size of 256 × 256, slice thickness of 1 mm and field of view (FOV) of 30 × 30 mm. Relative quantitative analysis of the signals was performed using ImageJ software. After the imaging experiments, the mice were euthanized, and grafts were obtained, paraffin sections were cut, and the sections were subjected to Perls' staining, H&E staining, immunofluorescence and IHC staining with HNA antibody (1:100, Abcam) to detect the hUC-MSC spheroids. Organs such as the liver, spleen, and kidney were also collected, cut into paraffin sections, and subjected to Perls' staining and H&E staining. Three mice per group were used for each experiment.

Statistical Analysis. All experiments were repeated 3 times independently, and all measurements were performed at least in triplicate. GraphPad software was used to conduct the statistical analyses. T test and one-way ANOVA were used to analyze differences between groups. The results are presented as the mean ± SD. $P < 0.05$ was considered statistically significant.

3. Results and discussion

Formation of human mesenchymal stem cell (hMSC) spheroids using a biomimetic hydrogel platform and labeling with ferumoxytol. Modulation of the physical properties of the cellular microenvironment can dynamically alter the growth pattern of cells [48]. Our previous studies have demonstrated that the growth of MIN6 pancreatic β-cells can be effectively altered by modulating the Young's modulus and stress relaxation of hydrogels [40]. However, different cell lines respond differently to the physical microenvironment. Composite hydrogels with tunable physical properties can meet the needs of various types of cells, and we have reported the use of such hydrogels for the three-dimensional culture of a variety of cells [40,49,50]. We designed two types of GelMA/PEGDA composite hydrogels for culturing human umbilical cord mesenchymal stem cell (hUC-MSCs) by adjusting the ratio of GelMA to PEGDA. We named the hydrogels multicellular spheroid (MCS)-culturing hydrogels and monolayer cell (MLC)-culturing hydrogels. After being cultured for three days, hUC-MSCs seeded on the two types of hydrogels showed different morphologies (Figs. S2A and B). The Young's modulus and stress relaxation of the two types of hydrogels were measured using a nanoindenter, and the Young's modulus and stress relaxation time ($t_{1/2}$) were calculated by stress-strain and stress-time curves, respectively. The results showed that the hydrogel stress relaxation time of the MCS-culturing hydrogels was 2.22 ± 0.83 s and Young's modulus reached 313.13 ± 6.56 kPa (Figs. S2C and D), while the MLC-culturing hydrogels showed a longer stress relaxation time and higher Young's modulus (data not shown). The apparent difference in the mechanical properties of the two types of biomimetic hydrogels led to a difference in the cellular microenvironment and further modulation of cell morphology.

Although ferumoxytol has potential clinical application as an MRI

contrast agent, its safety in labeling hUC-MSCs has not been fully investigated. Cell cytotoxicity experiment have showed that hUC-MSCs maintained a survival rate of greater than 90% when incubated with ferumoxytol up to 500 μg mL^{-1} for 5 days (Fig. S3A). Flow cytometric data also demonstrated ferumoxytol did not lead to significant apoptosis (Fig. S3B). In the next step, hUC-MSC spheroids were cultured on MCS-culturing hydrogels, and ferumoxytol was added at a concentration of 500 μg mL^{-1} during culture for spheroids labeling. The spheroid formation process of cells cultured at the same site on the MCS-culturing hydrogels was recorded by microscopy (Fig. 1B). Two hours after cell seeding, the cells started to respond to the physical microenvironment of the hydrogels, subsequently began to aggregate and formed a spherical

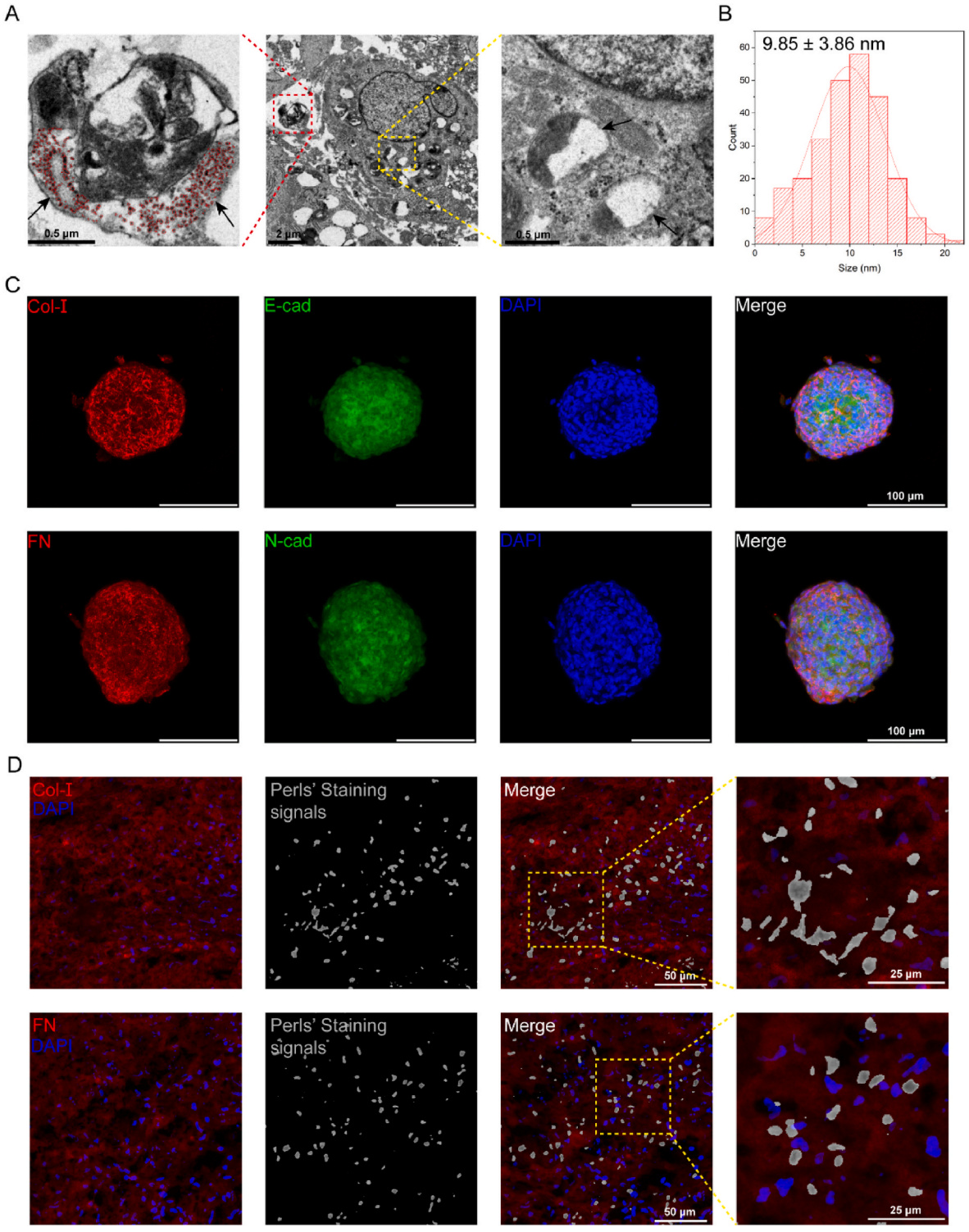

Fig. 2. Determination of ferumoxytol localization in spheroids. (A) TEM images of ferumoxytol-labeled spheroids. The left and right images are enlargements of the middle image. Left: extracellular; right: intracellular. The red dots represent the aggregates of ferumoxytol. (B) Size distribution of ferumoxytol in Fig. 2A. (C) Expression of the ECM proteins Col-I, FN (red staining) and E/N-cad (green staining); blue staining represents DAPI-positive nuclei. (D) Immunofluorescence staining of Col-I, FN (red staining) and Perls' staining of spheroids (grayscale plot of Perl's staining signals) in cryosections.

structure within 20 h. After labeling for three days, the structure of spheroids is more intact (Fig. 1C). Calculation of spheroid size revealed that the mean size of hUC-MSC spheroids were 117.3 ± 36.8 μm (Fig. 1D). The numbers of cells composed the spheroids with different ranges of size were counted after the spheroids being dissociated by trypsinization. Under a seeding density of 1 × 10^5 cells per cm^2 described in methods, the numbers of cells in spheroids of various size of spheroids (< 100 μm, 100–150 μm and 150–200 μm) were 128 ± 30, 265 ± 16, 599 ± 59 cells, respectively (Fig. S4A). Perls' staining of the labeled spheroids showed Prussian blue signals within the spheroids (Fig. 1E and F), indicating that ferumoxytol had been successfully encapsulated into spheroids. At the same time, different sizes of spheroids showed Perls' staining signals, and the signals were enhanced following the increasing size of spheroids (Fig. S4B).

Localization of ferumoxytol in spheroids after labeling. Previous research has illustrated that hUC-MSCs cannot take up ferumoxytol (Figs. S5A and B) under 2D-culture conditions. To determine whether the nanoparticles were localized in the intracellular or extracellular space in the spheroids, we digested the spheroids into single cells and performed Perls' staining and scanning transmission electron microscopy (TEM). No obvious nanoparticle aggregates were found in the cytoplasm (Figs. S5C and D). In addition, TEM analysis of spheroids demonstrated the absence of accumulated ferumoxytol within the cytoplasm of cells, while aggregates of ferumoxytol were found in intercellular spaces (Fig. 2A). These results indicated that our novel spheroid labeling method is independent of cellular uptake of ferumoxytol but relies on accumulation of ferumoxytol in the intercellular space. Meanwhile, TEM images revealed that ferumoxytol retained diameter of approximately 9.85 ± 3.86 nm (Fig. 2B), suggesting good stability of encapsulated nanoparticles in the spheroids.

Previous studies have reported that increased expression of the cellular communication proteins cadherins promotes enhanced intercellular interactions and tight junctions [39]. Our immunofluorescence staining results showed abundant expression of E/N-cadherin (E/N-cad) within MSC spheroids, while the abundant ECM proteins collagen I (Col-I) and fibronectin (FN) formed a complex compact network

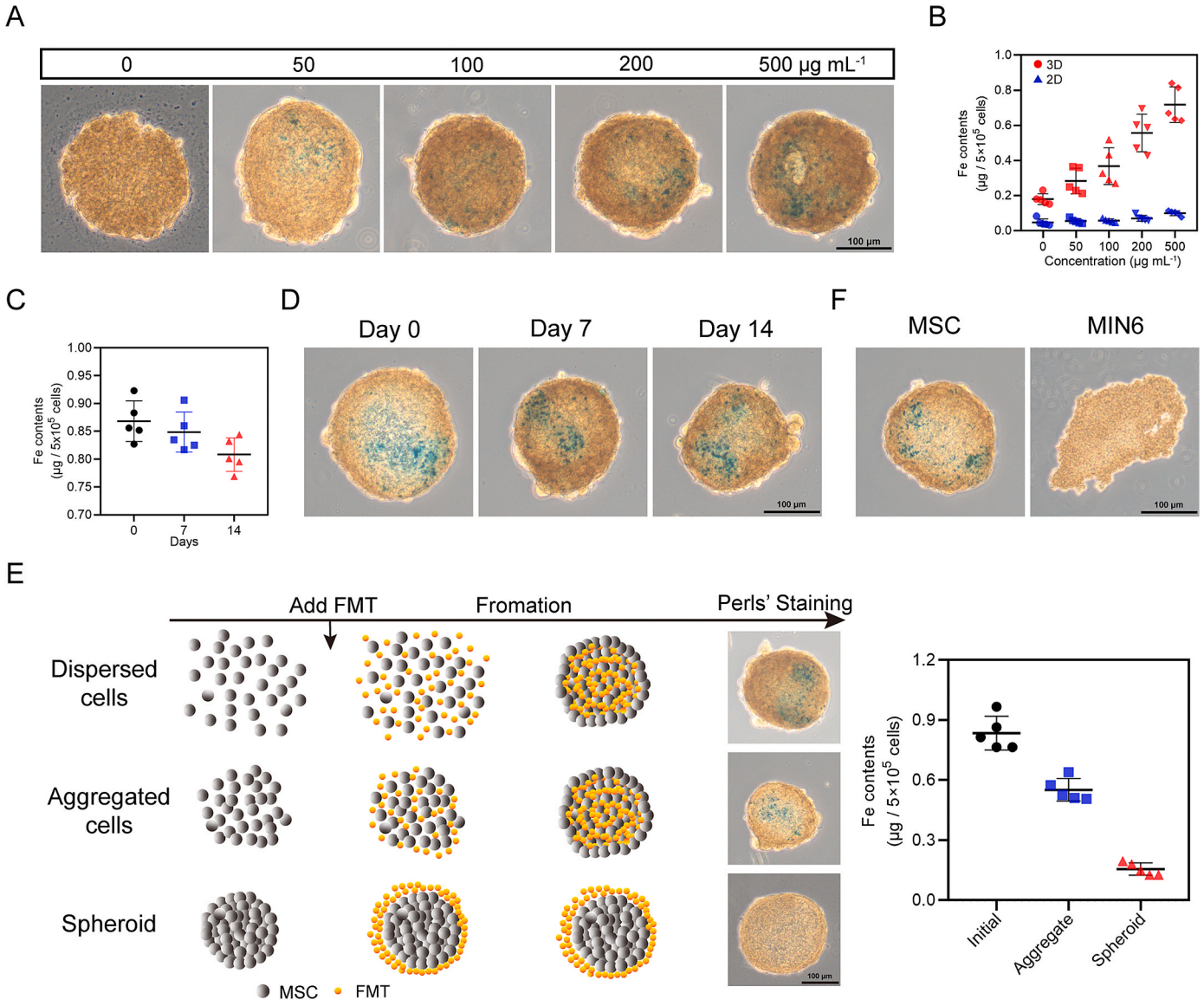

Fig. 3. Analysis of iron content during labeling processes. (A) Perls' staining of spheroids incubated with ferumoxytol at concentrations of 0, 50, 100, 200 and 500 μg mL^{-1} after labeling. (B) Measurement of iron content in spheroids and monolayer cells by ICP-MS. (C) ICP-MS analysis of iron content during 14 days culture after labeled. (D) Perls' staining of labeled spheroids after 0, 7 and 14 days of *in vitro* osteogenesis induction. (E) Perls' staining and ICP-MS analysis of spheroids when ferumoxytol was added in different phases of spheroids formation processes. (F) Perls' staining of hUC-MSC spheroids and pancreatic β-cells MIN6 aggregates labeled with ferumoxytol.

structure within cells (Fig. 2C). Since our labeling method does not involve cellular uptake of ferumoxytol, we suspected that ferumoxytol were trapped within tight junctions and associated with abundant ECM proteins, preventing the release and degradation of ferumoxytol. Immunofluorescence staining and Perls' staining of ECM proteins using frozen sections revealed that ferumoxytol was distributed in the ECM protein network composed of Col-I and fibronectin (Fig. 2D). Taken together, these results suggested that ferumoxytol was localized in the intercellular space and interacted with ECM proteins inside the spheroids, possibly ensuring their stable encapsulation.

Qualitative and quantitative analysis of labeling. To control the encapsulated iron content of ferumoxytol in spheroids, we quantified the iron content when different concentrations of ferumoxytol were added. We found that spheroids were labeled at ferumoxytol concentrations from 50 to 500 μg mL^{-1} and that the amount of ferumoxytol loaded into spheroids can be improved with increasing concentration (Fig. 3A). Accurate measurement of iron content using inductively coupled plasma-mass spectrometry (ICP-MS) (Fig. 3B) also revealed that the amount of ferumoxytol loaded in spheroids obtained from the same number of cell (5×10^5 cells) increased linearly with different ferumoxytol concentration, whereas there was little variation in iron content regardless of the ferumoxytol concentration in cells cultured under normal 2D conditions (Fig. 3B), due to the inability of hUC-MSCs to take up ferumoxytol (Figs. S5A and B) [27]. Notably, previously described MSC labeling methods using modified SPIONs or transfection reagent-treated ferumoxytol usually achieve an intracellular iron content of 10–40 pg per cell, which is equivalent to a total iron content of 5–20 μg for 5×10^5 cells [21,23,51]. The results indicated that the total iron content loaded by our 3D culture method was much lower than that achieved by cellular uptake of ferumoxytol (Fig. 3B), indicating that our method may eliminate the need for potentially cytotoxic ferumoxytol [32].

To explore whether the labeling was stable *in vitro*, elution amount of ferumoxytol from spheroids was measured after labeling. ICP-MS analysis showed the stable iron content during 14 days culture (Fig. 3C). Similarly, Perl's staining showed that the encapsulated iron was maintained inside the spheroids when induced with osteogenic differentiation culture medium for 2 weeks (Fig. 3D), confirming that this labeling method is stable and durable.

The spheroid formation processes involve initially loose aggregates and later compact cell spheroids induced by cell-cell/ECM interactions [39]. The addition of ferumoxytol at different phases of the spheroid's formation processes may affect the labeling efficiency. Thus, we added ferumoxytol for labeling at different phases according to Fig. 1B and found that when cells have formed compact spheroids, ferumoxytol could not effectively labeled spheroids, while when the cells were in a dispersed state or loose aggregates, ferumoxytol could loaded into the final spheroids (Fig. 3E). These results indicated that the labeling process is synchronized with the formation of spheroids. Different cell types with variable ECM proteins and cadherins may form different 3D structures [52]. We assembled 3D structures of different cell types (i.e., hUC-MSC and pancreatic β-cells MIN6) in different hydrogels. Unlike hUC-MSCs, MIN6 can only form loose aggregated patterns consistent with typical phenotypic characteristics of islets (Fig. 3F) and no Perls' staining signals within MIN6 aggregates. These results suggested the compact spheroid structure determines whether the labeling is successful.

Biosafety and function of magnetic labeling of hUC-MSC spheroids. To verify whether this labeling method affects cell activity, we evaluated the biosafety and function of labeled spheroids using higher concentrations of ferumoxytol (500 μg mL^{-1}). A large number of studies have shown that ferumoxytol composed of Fe(ii) and Fe(iii) can generate reactive oxygen species (ROS) through the Fenton reaction [53]. Excessive amounts of ROS can affect cell viability. We examined the intracellular ROS levels by DCFH-DA. The results showed that encapsulation of ferumoxytol did not cause excessive ROS accumulation (Fig. 4A), which may have been attributed to the absence of excessive accumulated ferumoxytol within the cells. Meanwhile, the ROS production was suppressed in spheroids compared to 2D-cultured hUC-MSCs. Previous studies have reported that the interior of spheroids is in a low-oxygen and low-nutrient environment [54,55], and reducing the onset of spheroid necrosis is one of the keys for ensuring the advantageousness of the 3D culture approach. By live-dead staining, we confirmed that the cell in spheroids prepared by MCS-culturing hydrogels could be maintained alive as in 2D-culture condition, and that ferumoxytol labeling had no significant effects on cell viability (Fig. 4B).

In addition, we also tested whether this labeling method has an effect on hUC-MSC functions. The colony-forming unit-fibroblast (CFU–F) assay showed that cells in spheroids maintained a higher self-renewal capacity (Fig. 4C and D). Flow cytometry analysis revealed no significant change in the levels of highly expressed surface markers, while the expression of CD14, CD19, CD34, CD45, and HLA-DR remained low (Fig. 4E). hUC-MSCs have differentiation potential, and loss of stemness gene expression often affects the ability of cells to differentiate [56]. We examined the expression of the stemness-related genes, OCT4, NANOG, and SOX2, and the results suggested that ferumoxytol did not significantly affect the expression of these genes; furthermore, labeled spheroids exhibited better differentiation ability, which is also consistent with previous results (Fig. 4F and G). Finally, we also examined osteogenic, adipogenic and chondrogenic differentiation. Alizarin red staining, Oil Red O staining and Alcian Blue staining indicated that the labeled spheroids maintained three lineages differentiation ability (Fig. 4H). Quantitative analysis of differentiation efficiency in Fig. S6 showed enhanced osteogenic and adipogenic differentiation capacity. All these results confirmed that cell viability and stemness were maintained well after use of our novel labeling method, while hUC-MSC functions were improved by the 3D culture technique.

***In vitro* and *in vivo* MRI monitoring of magnetic spheroids.** To investigate whether the magnetic spheroids prepared by our labeling method are suitable for MRI monitoring, we used 7.0 T MRI to scan the labeled spheroids and found apparent T2 signals (Fig. 5A and Fig. S7A). However, such signals were not detected under classical 2D-culture conditions at the same concentrations of ferumoxytol (Fig. S7B), which is consistent with our previous results. As expected, the T2 MRI signal was enhanced with increasing ferumoxytol concentration (Fig. 5B), which also resulted from differences in iron content inside the cell spheroids (Fig. 3A and B). Taken together, our results demonstrated that when cultured at same concentration of ferumoxytol, spheroids can achieve significantly enhanced T2 MRI signals as compared to 2D culture cells.

The above *in vitro* experiments demonstrated that ferumoxytol-labeled magnetic spheroids can be imaged by MRI. In addition, we further evaluated the ability of labeled spheroids to be monitored by *in vivo* tracking after transplantation. In general, magnetic spheroids were prepared using Dil-prelabeled hUC-MSCs under 500 μg mL^{-1} of ferumoxytol. Mixed magnetic spheroids with Matrigel and subcutaneously transplanted into the subaxillae of BALB/c nude mice, and the mice were subjected to T2-weighted MR scan at different days after transplantation (Fig. 5C). Fluorescence staining confirmed the presence of hUC-MSCs within the grafts (Fig. S8), and the MRI results revealed obvious T2 signals maintained up to 7 days (Fig. 5D). After 10 days of transplantation, the signal was mostly undetectable. Consistently, photographs of the grafts revealed a significant reduction of graft volume at Day 10 (Fig. S9A), and human nuclear antigen (HNA) IHC staining showed less HNA-positive signals in the grafts at Day 10 (Fig. S9B). This may be related to the significant shrinkage of the graft and the disruption of MSC spheroids integrity due to the migration of MSCs and the absorption of host. Histological analysis of the grafts demonstrated no significant inflammatory cell infiltration and a significant amount of iron accumulation (Fig. 5E). Unlabeled hUC-MSC spheroids have no T2 signals and Perls' staining signals (Fig. S10). In addition, we evaluated the *in vivo* viability of labeled spheroids and whether the release of

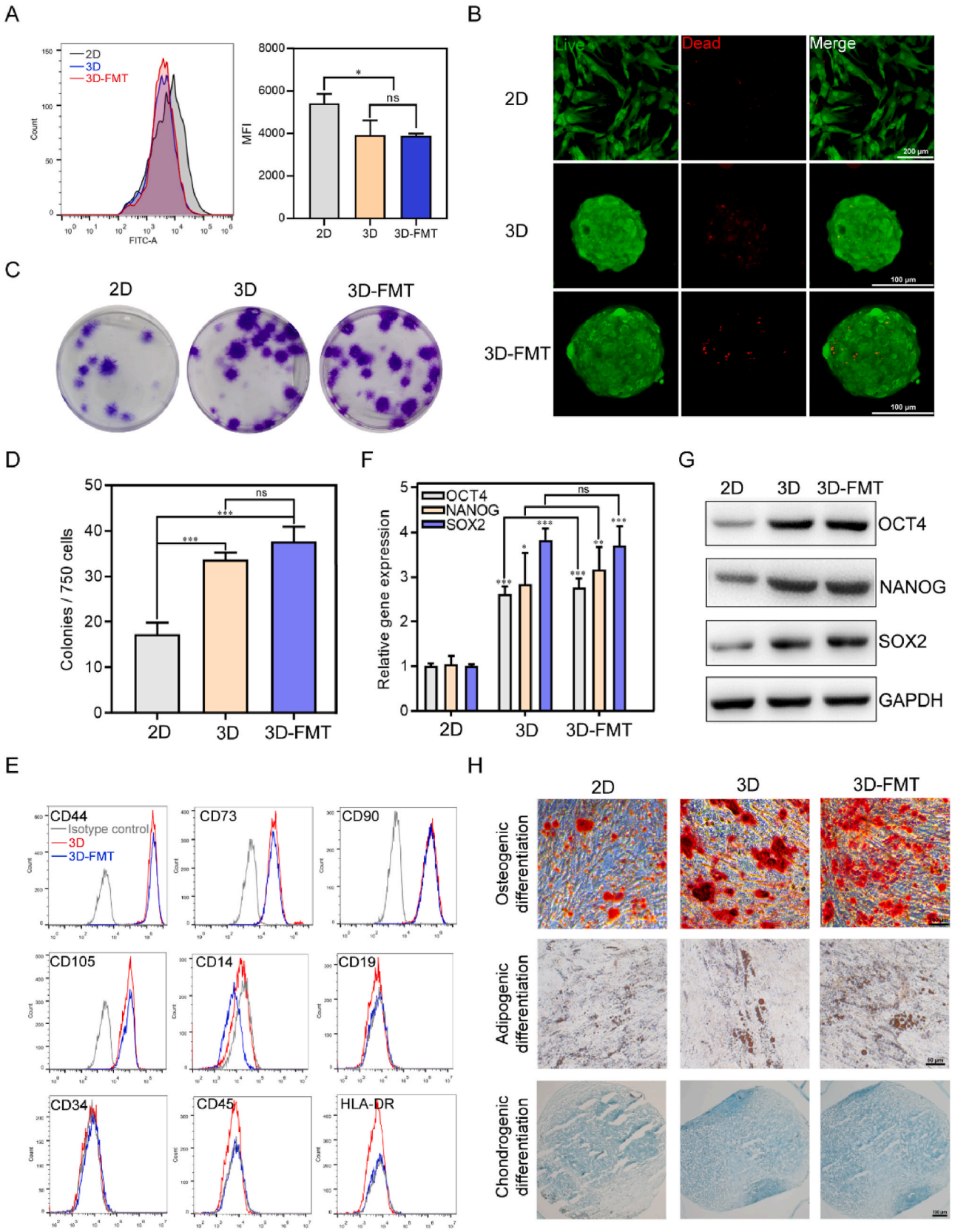

Fig. 4. Bioactivity and functional characterization of ferumoxytol-labeled spheroids. (A) Flow cytometry detection of cellular ROS levels and Median Fluorescence Intensity (MFI) of 2D-cultured hUC-MSCs (2D), spheroids (3D) and ferumoxytol-labeled spheroids (3D-FMT). (B) Representative image of live/dead staining; green- and red-labeled cells are living and dead cells, respectively. (C) Crystal violet staining showing colony formation and (D) statistical analysis of the number of clones. (E) Analysis of surface biomarker levels in spheroids by flow cytometry. (F) The mRNA expression levels and (G) the protein expression levels of OCT4, NANOG and SOX2 in spheroids. (H) Alizarin red (top), Oil Red O (middle) and Alcian Blue staining (bottom) of spheroids cultured in differentiation induction medium. Values are mean ± SD, no significance (ns), $^{*}P < 0.05$, $^{**}P < 0.01$, $^{***}P < 0.001$ vs. 2D.

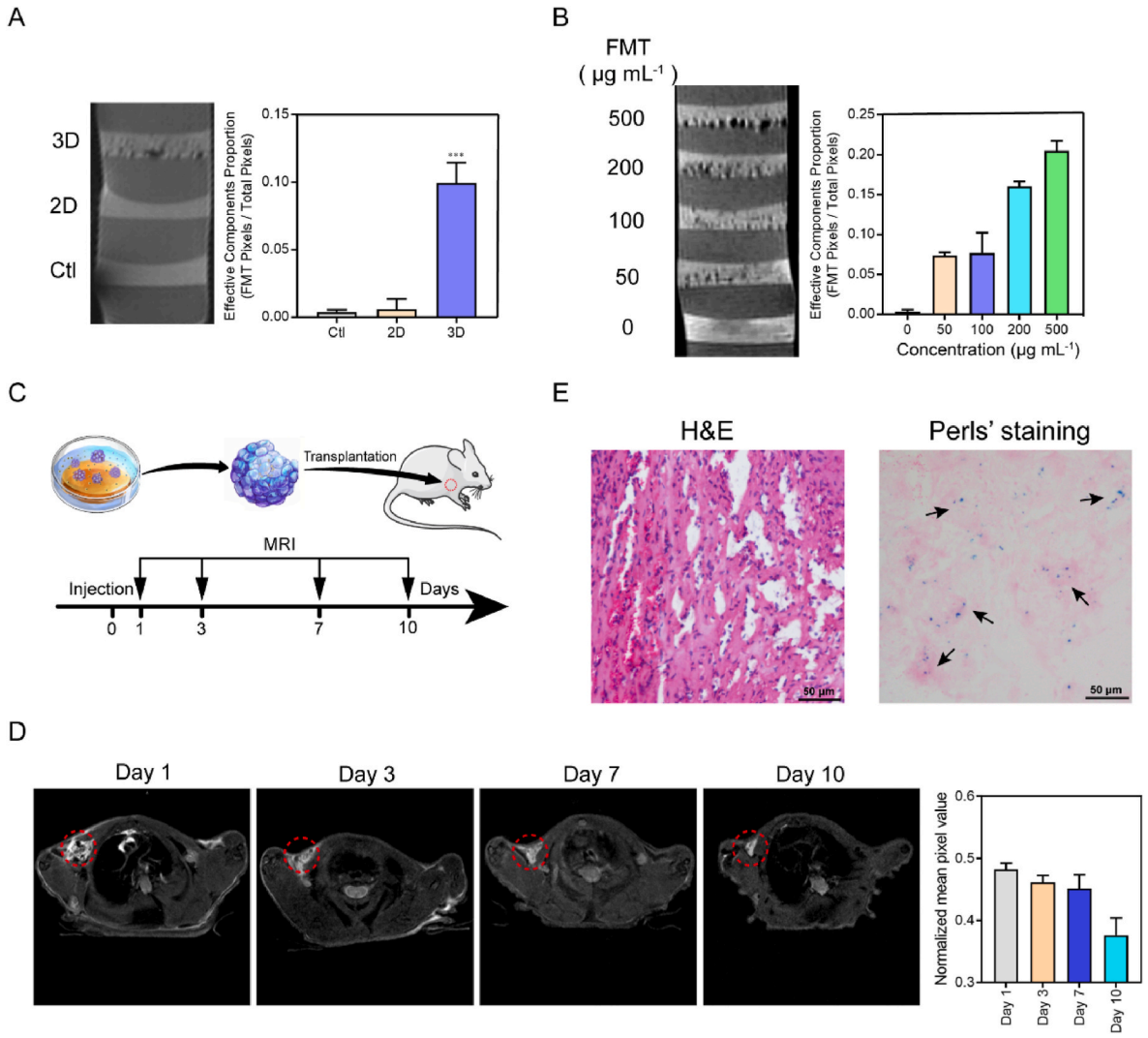

Fig. 5. *In vitro* and *in vivo* MRI of ferumoxytol-labeled spheroids. (A) Longitudinal T2 MRI sections of agarose containing cells cultured on different hydrogels and relative quantitative analysis. (B) T2 MR images of spheroids incubated with 0, 50, 100, 200 and 500 μg mL^{-1} of ferumoxytol and relative quantitative analysis. (C) Experimental protocol for MRI tracking post-transplantation in BALB/c nude mice. (D) Axial T2 MR images of mice at 1, 3, 7, and 10 days after transplanted with labeled hUC-MSC spheroid and relative quantitative analysis. (E) Perls' staining (right) and H&E staining (left) sections of grafts. Arrows represent Prussian blue signals.

ferumoxytol post-transplantation had an effect on organs. In Fig. S11, there was no difference of TUNEL-positive signals between labeled and unlabeled spheroids, both of which were lower than that of 2D-cultured cells injected into mice. H&E staining and Perls' staining of tissue sections of the liver, kidney and spleen showed no significant tissue damage or iron accumulation (Fig. S12).

4. Conclusion

In summary, we established a novel method for extracellular labeling of MSC spheroids using clinically approved magnetic nanomaterials, which allows MRI tracking of MSC spheroids after transplantation. This approach enables bottom-up assembly of MSCs to form spheroids using a biomimetic hydrogel with tunable physical properties and clinical-grade ferumoxytol for labeling, allowing ferumoxytol to label the interior of the spheroids during cellular self-organization without internalization by individual cells. Our method is independent on the modification of ferumoxytol by transfection reagents, which can enhance the reproducibility. Low doses of ferumoxytol inside the spheroids can achieve strong MRI sensitivity, which causes nontoxic effect to MSCs. In addition, the magnetic spheroids generated during ferumoxytol labeling retain the advantages of spheroids in terms of cell proliferation, stemness maintenance, and differentiation capacity. The safe and effective labeling method proposed in this work can also be used for MRI tracking of MSC spheroids post-transplantation to determine whether transplantation was successful and evaluate the retention time of spheroids in damaged tissues, which may provide important information for the development of MSC-mediated regenerative medicine.

Ethics approval and consent to participate

Human umbilical cord mesenchymal stem cells (hUC-MSCs) were obtained from the Clinical Stem Cell Center of the Nanjing Drum Tower Hospital (China). Informed consent was obtained from all volunteers, and ethical approval was obtained from the Ethics Committee of Drum Tower Hospital Affiliated to the Medical School of Nanjing University (No. 2017-161-06). All *in vivo* experiments were performed according to the guidelines of the Animal Care & Welfare Committee of Southeast University (No. 20210526003).

CRediT authorship contribution statement

Sen Yan: Conceptualization, Methodology, Investigation, Formal analysis, Writing – original draft. **Ke Hu:** Conceptualization, Funding acquisition, Formal analysis, Writing – original draft. **Miao Zhang:** Methodology, Investigation, Formal analysis, Writing – review & editing. **Jingyi Sheng:** Formal analysis, Writing – review & editing. **Xueqin Xu:** Investigation, Formal analysis, Validation, Resources. **Shijia Tang:** Investigation, Formal analysis, Validation. **Yan Li:** Resources, Writing – review & editing. **Sheng Yang:** Investigation, Visualization. **Guangxiang Si:** Investigation. **Yu Mao:** Investigation. **Yi Zhang:** Resources. **Feimin Zhang:** Supervision, Funding acquisition. **Ning Gu:** Supervision, Funding acquisition, Project administration.

Declaration of competing interest

All authors declare that they have no conflict of interest.

Acknowledgements

This work was supported by the National Key Research and Development Program of China (2017YFA0104302), the National Natural Science Foundation of China (51832001, 61821002, 81870807), the China Postdoctoral Science Foundation (2017M621787), and the Talent Introduction Foundation of Nanjing Medical University (2017RC07). The authors thank Fengchao Zang of Southeast University for help with 7.0 T MRI, Yuanyuan Xie of Nanjing Drum Tower Hospital for help with the detection of hUC-MSC surface markers, Zhaobin Guo of Johns Hopkins University for editing of the manuscript and Tingting Yu of Nanjing Medical University for discussions of this work.

Appendix A. Supplementary data

Supplementary data to this article can be found online at https://doi.org/10.1016/j.bioactmat.2022.04.024.

References

[1] G. Chamberlain, J. Fox, B. Ashton, J. Middleton, Concise review: mesenchymal stem cells: their phenotype, differentiation capacity, immunological features, and potential for homing, Stem Cell. 25 (11) (2007) 2739–2749.
[2] M.F. Pittenger, D.E. Discher, B.M. Peault, D.G. Phinney, J.M. Hare, A.I. Caplan, Mesenchymal stem cell perspective: cell biology to clinical progress, NPJ Regen Med 4 (2019) 22.
[3] Y. Shi, Y. Wang, Q. Li, K. Liu, J. Hou, C. Shao, Y. Wang, Immunoregulatory mechanisms of mesenchymal stem and stromal cells in inflammatory diseases, Nat. Rev. Nephrol. 14 (8) (2018) 493–507.
[4] G. Upadhyay, S. Shankar, R.K. Srivastava, Stem cells in neurological disorders: emerging therapy with stunning hopes, Mol. Neurobiol. 52 (1) (2015) 610–625.
[5] O. Honmou, K. Houkin, T. Matsunaga, Y. Niitsu, S. Ishiai, R. Onodera, S. G. Waxman, J.D. Kocsis, Intravenous administration of auto serum-expanded autologous mesenchymal stem cells in stroke, Brain 134 (Pt 6) (2011) 1790–1807.
[6] J. Chen, C.X. Zheng, Y. Jin, C.H. Hu, Mesenchymal stromal cell-mediated immune regulation: a promising remedy in the therapy of type 2 diabetes mellitus, Stem Cell. 39 (7) (2021) 838–852.
[7] J. Liu, D. Han, Z. Wang, M. Xue, L. Zhu, H. Yan, X. Zheng, Z. Guo, H. Wang, Clinical analysis of the treatment of spinal cord injury with umbilical cord mesenchymal stem cells, Cytotherapy 15 (2) (2013) 185–191.
[8] J.J. Hwang, Y.A. Rim, Y. Nam, J.H. Ju, Recent developments in clinical applications of mesenchymal stem cells in the treatment of rheumatoid arthritis and osteoarthritis, Front. Immunol. 12 (2021) 631291.
[9] R. El Omar, J. Beroud, J.F. Stoltz, P. Menu, E. Velot, V. Decot, Umbilical cord mesenchymal stem cells: the new gold standard for mesenchymal stem cell-based therapies? Tissue Eng. B Rev. 20 (5) (2014) 523–544.
[10] J. Bartolucci, F.J. Verdugo, P.L. Gonzalez, R.E. Larrea, E. Abarzua, C. Goset, P. Rojo, I. Palma, R. Lamich, P.A. Pedreros, G. Valdivia, V.M. Lopez, C. Nazzal, F. Alcayaga-Miranda, J. Cuenca, M.J. Brobeck, A.N. Patel, F.E. Figueroa, M. Khoury, Safety and efficacy of the intravenous infusion of umbilical cord mesenchymal stem cells in patients with heart failure: a phase 1/2 randomized controlled trial (RIMECARD trial [randomized clinical trial of intravenous infusion umbilical cord mesenchymal stem cells on cardiopathy]), Circ. Res. 121 (10) (2017) 1192–1204.
[11] B.H. Lee, J.N. Park, E.J. Lee, Y.W. Moon, J.H. Wang, Therapeutic efficacy of spherical aggregated human bone marrow-derived mesenchymal stem cells cultured for osteochondral defects of rabbit knee joints, Am. J. Sports Med. 46 (9) (2018) 2242–2252.
[12] M.J. Hoogduijn, M.G. Betjes, C.C. Baan, Mesenchymal stromal cells for organ transplantation: different sources and unique characteristics? Curr. Opin. Organ Transplant. 19 (1) (2014) 41–46.
[13] Y. Xia, J. Sun, L. Zhao, F. Zhang, X.J. Liang, Y. Guo, M.D. Weir, M.A. Reynolds, N. Gu, H.H.K. Xu, Magnetic field and nano-scaffolds with stem cells to enhance bone regeneration, Biomaterials 183 (2018) 151–170.
[14] Y.T. He, X.L. Zhu, S.F. Li, B.Q. Zhang, Y. Li, Q. Wu, Y.L. Zhang, Y.Y. Zhou, L. Li, Y. N. Qi, J. Bao, H. Bu, Creating rat hepatocyte organoid as an in vitro model for drug testing, World J. Stem Cell. 12 (10) (2020) 1184–1195.
[15] M.R. Bernsen, A.D. Moelker, P.A. Wielopolski, S.T. van Tiel, G.P. Krestin, Labelling of mammalian cells for visualisation by MRI, Eur. Radiol. 20 (2) (2010) 255–274.
[16] S.M. Dadfar, K. Roemhild, N.I. Drude, S. von Stillfried, R. Knuchel, F. Kiessling, T. Lammers, Iron oxide nanoparticles: diagnostic, therapeutic and theranostic applications, Adv. Drug Deliv. Rev. 138 (2019) 302–325.
[17] Z. Zhou, L. Yang, J. Gao, X. Chen, Structure-relaxivity relationships of magnetic nanoparticles for magnetic resonance imaging, Adv. Mater. 31 (8) (2019), e1804567.
[18] C. Ansari, G.A. Tikhomirov, S.H. Hong, R.A. Falconer, P.M. Loadman, J.H. Gill, R. Castaneda, F.K. Hazard, L. Tong, O.D. Lenkov, D.W. Felsher, J. Rao, H. E. Daldrup-Link, Development of novel tumor-targeted theranostic nanoparticles activated by membrane-type matrix metalloproteinases for combined cancer magnetic resonance imaging and therapy, Small 10 (3) (2014) 566–575, 417.
[19] D. Berner, W. Brehm, K. Gerlach, C. Gittel, J. Offhaus, F. Paebst, D. Scharner, J. Burk, Longitudinal cell tracking and simultaneous monitoring of tissue regeneration after cell treatment of natural tendon disease by low-field magnetic resonance imaging, Stem Cell. Int. 2016 (2016) 1207190.
[20] N. Guldris, B. Argibay, J. Gallo, R. Iglesias-Rey, E. Carbo-Argibay, Y.V. Kolen'ko, F. Campos, T. Sobrino, L.M. Salonen, M. Banobre-Lopez, J. Castillo, J. Rivas, Magnetite nanoparticles for stem cell labeling with high efficiency and long-term in vivo tracking, Bioconjugate Chem. 28 (2) (2017) 362–370.
[21] K. Andreas, R. Georgieva, M. Ladwig, S. Mueller, M. Notter, M. Sittinger, J. Ringe, Highly efficient magnetic stem cell labeling with citrate-coated superparamagnetic iron oxide nanoparticles for MRI tracking, Biomaterials 33 (18) (2012) 4515–4525.
[22] Jasmin, A.L. Torres, L. Jelicks, A.C. de Carvalho, D.C. Spray, R. Mendez-Otero, Labeling stem cells with superparamagnetic iron oxide nanoparticles: analysis of the labeling efficacy by microscopy and magnetic resonance imaging, Methods Mol. Biol. 906 (2012) 239–252.
[23] F. Schulze, A. Dienelt, S. Geissler, P. Zaslansky, J. Schoon, K. Henzler, P. Guttmann, A. Gramoun, L.A. Crowe, L. Maurizi, J.P. Vallee, H. Hofmann, G.N. Duda, A. Ode, Amino-polyvinyl alcohol coated superparamagnetic iron oxide nanoparticles are suitable for monitoring of human mesenchymal stromal cells in vivo, Small 10 (21) (2014) 4340–4351.
[24] I.C. Macdougall, W.E. Strauss, J. McLaughlin, Z. Li, F. Dellanna, J. Hertel, A randomized comparison of ferumoxytol and iron sucrose for treating iron deficiency anemia in patients with CKD, Clin. J. Am. Soc. Nephrol. 9 (4) (2014) 705–712.
[25] A. Khurana, F. Chapelin, G. Beck, O.D. Lenkov, J. Donig, H. Nejadnik, S. Messing, N. Derugin, R.C. Chan, A. Gaur, B. Sennino, D.M. McDonald, P.J. Kempen, G. A. Tikhomirov, J. Rao, H.E. Daldrup-Link, Iron administration before stem cell harvest enables MR imaging tracking after transplantation, Radiology 269 (1) (2013) 186–197.
[26] A.S. Arbab, G.T. Yocum, H. Kalish, E.K. Jordan, S.A. Anderson, A.Y. Khakoo, E. J. Read, J.A. Frank, Efficient magnetic cell labeling with protamine sulfate complexed to ferumoxides for cellular MRI, Blood 104 (4) (2004) 1217–1223.
[27] M.S. Thu, L.H. Bryant, T. Coppola, E.K. Jordan, M.D. Budde, B.K. Lewis, A. Chaudhry, J. Ren, N.R. Varma, A.S. Arbab, J.A. Frank, Self-assembling nanocomplexes by combining ferumoxytol, heparin and protamine for cell tracking by magnetic resonance imaging, Nat. Med. 18 (3) (2012) 463–467.
[28] P. Wang, S. Ma, G. Ning, W. Chen, B. Wang, D. Ye, B. Chen, Y. Yang, Q. Jiang, N. Gu, J. Sun, Entry-prohibited effect of kHz pulsed magnetic field upon interaction between SPIO nanoparticles and mesenchymal stem cells, IEEE Trans. Biomed. Eng. 67 (4) (2020) 1152–1158.
[29] A. Ohki, S. Saito, K. Fukuchi, Magnetic resonance imaging of umbilical cord stem cells labeled with superparamagnetic iron oxide nanoparticles: effects of labelling and transplantation parameters, Sci. Rep. 10 (1) (2020) 13684.
[30] N. Singh, G.J. Jenkins, R. Asadi, S.H. Doak, Potential toxicity of superparamagnetic iron oxide nanoparticles (SPION), Nano Rev. 1 (2010).
[31] S. Ghosh, I. Ghosh, M. Chakrabarti, A. Mukherjee, Genotoxicity and biocompatibility of superparamagnetic iron oxide nanoparticles: influence of surface modification on biodistribution, retention, DNA damage and oxidative stress, Food Chem. Toxicol. 136 (2020) 110989.
[32] G. Liu, J. Gao, H. Ai, X. Chen, Applications and potential toxicity of magnetic iron oxide nanoparticles, Small 9 (9–10) (2013) 1533–1545.
[33] Z. Cesarz, K. Tamama, Spheroid culture of mesenchymal stem cells, Stem Cell. Int. 2016 (2016) 9176357.
[34] S. Ezquerra, A. Zuleta, R. Arancibia, J. Estay, F. Aulestia, F. Carrion, Functional properties of human-derived mesenchymal stem cell spheroids: a meta-analysis and systematic review, Stem Cell. Int. 2021 (2021) 8825332.
[35] M. Madrigal, K.S. Rao, N.H. Riordan, A review of therapeutic effects of mesenchymal stem cell secretions and induction of secretory modification by different culture methods, J. Transl. Med. 12 (2014) 260.
[36] Y. Qiao, Z. Xu, Y. Yu, S. Hou, J. Geng, T. Xiao, Y. Liang, Q. Dong, Y. Mei, B. Wang, H. Qiao, J. Dai, G. Suo, Single cell derived spheres of umbilical cord mesenchymal

stem cells enhance cell stemness properties, survival ability and therapeutic potential on liver failure, Biomaterials 227 (2020) 119573.
[37] B. Jiang, L. Yan, Z. Miao, E. Li, K.H. Wong, R.H. Xu, Spheroidal formation preserves human stem cells for prolonged time under ambient conditions for facile storage and transportation, Biomaterials 133 (2017) 275–286.
[38] T.J. Bartosh, J.H. Ylostalo, A. Mohammadipoor, N. Bazhanov, K. Coble, K. Claypool, R.H. Lee, H. Choi, D.J. Prockop, Aggregation of human mesenchymal stromal cells (MSCs) into 3D spheroids enhances their antiinflammatory properties, Proc. Natl. Acad. Sci. U. S. A. 107 (31) (2010) 13724–13729.
[39] X. Cui, Y. Hartanto, H. Zhang, Advances in multicellular spheroids formation, J. R. Soc. Interface 14 (127) (2017).
[40] M. Zhang, S. Yan, X. Xu, T. Yu, Z. Guo, M. Ma, Y. Zhang, Z. Gu, Y. Feng, C. Du, M. Wan, K. Hu, X. Han, N. Gu, Three-dimensional cell-culture platform based on hydrogel with tunable microenvironmental properties to improve insulin-secreting function of MIN6 cells, Biomaterials 270 (2021) 120687.
[41] P.A. Janmey, R.T. Miller, Mechanisms of mechanical signaling in development and disease, J. Cell Sci. 124 (Pt 1) (2011) 9–18.
[42] O. Chaudhuri, L. Gu, D. Klumpers, M. Darnell, S.A. Bencherif, J.C. Weaver, N. Huebsch, H.P. Lee, E. Lippens, G.N. Duda, D.J. Mooney, Hydrogels with tunable stress relaxation regulate stem cell fate and activity, Nat. Mater. 15 (3) (2016) 326–334.
[43] D. Kouroupis, D. Correa, Increased mesenchymal stem cell functionalization in three-dimensional manufacturing settings for enhanced therapeutic applications, Front. Bioeng. Biotechnol. 9 (2021) 621748.
[44] A.J. Theruvath, H. Nejadnik, O. Lenkov, K. Yerneni, K. Li, L. Kuntz, C. Wolterman, J. Tuebel, R. Burgkart, T. Liang, S. Felt, H.E. Daldrup-Link, Tracking stem cell implants in cartilage defects of minipigs by using ferumoxytol-enhanced MRI, Radiology 292 (1) (2019) 129–137.
[45] T.C. Tseng, S.H. Hsu, Substrate-mediated nanoparticle/gene delivery to MSC spheroids and their applications in peripheral nerve regeneration, Biomaterials 35 (9) (2014) 2630–2641.
[46] J. Schmehl, H. Stoll, M. Danalache, G.C. Grozinger, T.O. Greiner, R.F. Leibfritz, P. Martirosian, K. Nikolaou, S. Elser, Intravascular application of labelled cell spheroids: an approach for ischemic peripheral artery disease, Int. J. Mol. Sci. 22 (13) (2021).
[47] D. Fayol, G. Frasca, C. Le Visage, F. Gazeau, N. Luciani, C. Wilhelm, Use of magnetic forces to promote stem cell aggregation during differentiation, and cartilage tissue modeling, Adv. Mater. 25 (18) (2013) 2611–2616.
[48] K.H. Vining, D.J. Mooney, Mechanical forces direct stem cell behaviour in development and regeneration, Nat. Rev. Mol. Cell Biol. 18 (12) (2017) 728–742.
[49] S. Tang, K. Hu, J. Sun, Y. Li, Z. Guo, M. Liu, Q. Liu, F. Zhang, N. Gu, High quality multicellular tumor spheroid induction platform based on anisotropic magnetic hydrogel, ACS Appl. Mater. Interfaces 9 (12) (2017) 10446–10452.
[50] T.T. Yu, K. Hu, Q.F. Xu, X.Q. Xu, C.Y. Du, Y.Y. Zhao, S. Yan, W. Wang, S.J. Tang, S. Yue, X.Y. Zhang, D.L. Wang, F.M. Zhang, S.Y. Cheng, N. Gu, An easy-to-fabricate hydrogel platform with tunable stiffness and cell anchorage: validation of its feasibility in modulating sonic hedgehog signaling pathway physically, Macromol. Mater. Eng. 305 (4) (2020).
[51] G. Yang, W. Ma, B. Zhang, Q. Xie, The labeling of stem cells by superparamagnetic iron oxide nanoparticles modified with PEG/PVP or PEG/PEI, Mater Sci Eng C Mater Biol Appl 62 (2016) 384–390.
[52] A. Tocchio, N.G. Durmus, K. Sridhar, V. Mani, B. Coskun, R. El Assal, U. Demirci, Magnetically guided self-assembly and coding of 3D living architectures, Adv. Mater. 30 (4) (2018).
[53] V. Trujillo-Alonso, E.C. Pratt, H. Zong, A. Lara-Martinez, C. Kaittanis, M.O. Rabie, V. Longo, M.W. Becker, G.J. Roboz, J. Grimm, M.L. Guzman, FDA-approved ferumoxytol displays anti-leukaemia efficacy against cells with low ferroportin levels, Nat. Nanotechnol. 14 (6) (2019) 616–622.
[54] S. Riffle, R.N. Pandey, M. Albert, R.S. Hegde, Linking hypoxia, DNA damage and proliferation in multicellular tumor spheroids, BMC Cancer 17 (1) (2017) 338.
[55] F. Hirschhaeuser, H. Menne, C. Dittfeld, J. West, W. Mueller-Klieser, L.A. Kunz-Schughart, Multicellular tumor spheroids: an underestimated tool is catching up again, J. Biotechnol. 148 (1) (2010) 3–15.
[56] T. Ahmad, J. Lee, Y.M. Shin, H.J. Shin, S.K.M. Perikamana, S.H. Park, S.W. Kim, H. Shin, Hybrid-spheroids incorporating ECM like engineered fragmented fibers potentiate stem cell function by improved cell/cell and cell/ECM interactions, Acta Biomater. 64 (2017) 161–175.